Physical Modeling of Unsteady Turbulence in Breaking Tidal Bores

Nicholas J. Docherty[1] and Hubert Chanson[2]

Abstract: A tidal bore is an unsteady flow motion generated by the rapid water level rise at the river mouth during the early flood tide under macrotidal and appropriate bathymetric conditions. This paper presents a study that physically investigates the turbulent properties of tidal bores. Results from some experimental measurements of free-surface fluctuations and turbulent velocities conducted on smooth and rough beds are reported. The free-surface measurements were conducted with Froude numbers of 1–1.7. Both undular and breaking bores were observed. Using an ensemble-averaging technique, the free-surface fluctuations of breaking tidal bores are characterized. Immediately before the roller, the free-surface curves gradually upwards. The passage of the bore roller is associated with some large water elevation fluctuations; the largest free-surface fluctuations are observed during the first half of the bore roller. The turbulent velocity measurements were performed at several vertical elevations during and shortly after the passage of breaking bores. Both the instantaneous and ensemble-averaged velocity data highlight a strong flow deceleration at all elevations during the bore passage. Close to the bed, the longitudinal velocity component becomes negative immediately after the roller passage, implying the existence of a transient recirculation. The height and duration of the transient are a function of the bed roughness, with a higher and longer recirculation region above the rough bed. The vertical velocity data presented some positive, upward motion beneath the front with increasing maximum vertical velocity with increasing distance from the bed. The transverse velocity data show some large fluctuations with nonzero ensemble average after the roller passage that highlight some intense secondary motion advected behind the bore front. **DOI: 10.1061/(ASCE)HY.1943-7900.0000542.**

CE Database subject headings: Turbulence; Velocity; Unsteady flow; Water levels; Floods; Hydraulic models.

Author keywords: Breaking tidal bores; Turbulence; Physical modelling; Free-surface fluctuations; Ensemble-averaged velocity components.

Introduction

A tidal bore is an unsteady flow motion generated by the rapid water level rise at the river mouth during the early flood tide. With time, the leading edge of the tidal wave becomes steeper until it forms a wall of water (i.e., the tidal bore). After the formation of the bore, a discontinuity occurs in water depth and velocity field at the bore front (Fig. 1). Once formed, the flow properties immediately in front of and behind the tidal bore must satisfy the continuity and momentum principles (Rayleigh 1908; Henderson 1966; Liggett 1994; Chanson 2012). The integral form of the equations of conservation of mass and momentum gives some relationship between the flow properties in front of and behind the bore front. For an observer traveling at the surge speed U in a rectangular horizontal channel and neglecting bed friction, the quasi steady flow analogy yields:

$$\frac{d_{\text{conj}}}{d_o} = \frac{1}{2}\left(\sqrt{1+8\mathsf{F}^2}-1\right) \quad (1)$$

where d_o = initial water depth (Figs. 1 and 2); d_{conj} = downstream conjugate flow depth immediately after the bore passage (Fig. 1); V_o = initial river flow velocity positive downstream (Fig. 2); and U = tidal bore celerity for an observer standing on the bank positive upstream (Fig. 2). The tidal bore Froude number F is defined as:

$$\mathsf{F} = \frac{V_o + U}{\sqrt{g\ d_o}} \quad (2)$$

The tidal bore Froude number F is always greater than unity. For $\mathsf{F} < 1$, the tidal wave cannot transform into a tidal bore. The tidal bore front is a turbulent unsteady flow motion that is comparable with a shock (Lighthill 1978). Fig. 1 shows a small tidal bore.

Despite some recent advances (Hornung et al. 1995; Koch and Chanson 2009; Chanson 2010), knowledge of the unsteady turbulent motion in a tidal bore remains limited. This study physically investigates the turbulent flow properties of tidal bores. A some experimental measurements of free-surface fluctuations and turbulent velocities conducted in a relatively large facility on smooth and rough beds are analyzed. This paper characterizes the unsteady turbulent velocity fields in breaking tidal bores.

Physical Modeling of Tidal Bores

Presentation

Laboratory studies of tidal bores are performed with geometrically similar models for which the geometric scaling ratio L_r is defined as the ratio of prototype-to-model dimensions. Physical modeling requires the selection of an adequate similitude. For a tidal bore

[1]Research student, Univ. of Queensland, School of Civil Engineering, Brisbane QLD 4072, Australia.

[2]Professor in Hydraulic Engineering, Univ. of Queensland, School of Civil Engineering, Brisbane QLD 4072, Australia (corresponding author). E-mail: h.chanson@uq.edu.au

Note. This manuscript was submitted on July 27, 2010; approved on December 6, 2011; published online on December 8, 2011. Discussion period open until October 1, 2012; separate discussions must be submitted for individual papers. This paper is part of the ***Journal of Hydraulic Engineering***, Vol. 138, No. 5, May 1, 2012. ©ASCE, ISSN 0733-9429/2012/5-412–419/$25.00.

Fig. 1. Photograph of tidal bore of the Sélune River (France) on September, 2008 ($F \sim 1.4$–1.6, $R \sim 2 \times 10^6$); bore propagation from left to right

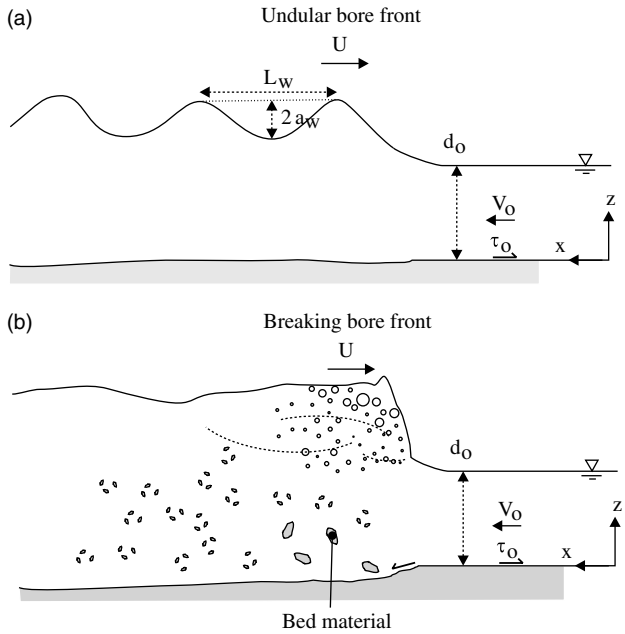

Fig. 2. Definition sketch of tidal bores: (a) undular bore propagating upstream; (b) riverbed scour beneath a breaking tidal bore

propagating in a horizontal, rectangular channel, a simplified dimensional analysis yields:

$$d, V_x, V_y, V_z = F_1(x, y, z, t, U, d_o, V_o, \delta, B, g, \rho, \mu, \sigma \ldots) \qquad (3)$$

where d = flow depth; V_x, V_y, V_z = respectively, the longitudinal, transverse, and vertical velocity components at a location (x, y, z); x = coordinate in the flow direction; y = horizontal transverse coordinate measured from the channel centerline; z = vertical coordinate measured from the channel bed; t = time; U = surge celerity; V_o = initial flow velocity; δ = boundary layer thickness at x; B = channel width; g = gravity acceleration; ρ and μ = water density and dynamic viscosity, respectively; and σ = surface tension between air and water. Eq. (3) expresses the flow properties (on the left) at a position (x, y, z) and at a time t as functions of the tidal bore properties, initial flow properties, channel geometry, and fluid properties. In addition, the biochemical properties of the water solution may be considered, especially in natural estuarine systems.

For a tidal bore, the theoretical considerations showed that the relevant characteristic length and velocity scales are, respectively, the initial flow depth d_o and $(V_o + U)$ [Eqs. (1) and (2)]. Eq. (3) may be rewritten in dimensionless terms

$$\frac{d}{d_o}, \frac{V_x}{V_o}, \frac{V_y}{V_o}, \frac{V_z}{V_o} = F_2\left[\frac{x}{d_o}, \frac{y}{d_o}, \frac{z}{d_o}, t\sqrt{\frac{g}{d_o}}, \frac{V_o + U}{\sqrt{g d_o}}, \rho \times \frac{(V_o + U)d_o}{\mu}, \frac{\delta}{d_o}, \frac{B}{d_o}, \frac{g\mu^4}{\rho\sigma^3}, \ldots\right] \qquad (4)$$

In Eq. (4), the fifth and sixth terms on the right are the tidal bore Froude and Reynolds numbers, respectively, and the ninth term is the Morton number, which is a function only of fluid properties and gravity constant.

In a geometrically similar model, a true dynamic similarity is achieved only if each dimensionless parameter has the same value in both model and prototype. Scale effects may exist when one or more terms have different values between the model and prototype. In free-surface flows, including tidal bores, the gravity effects are important, and a Froude similitude is commonly used (Henderson 1966; Chanson 1999). That is, the model and prototype Froude numbers must be equal. However, the turbulent mixing processes are dominated by viscous forces, implying the needs for a Reynolds similitude. Fig. 1 shows the turbulence of a tidal bore front. For geometrically similar tidal bore models, it is impossible to satisfy simultaneously all of the similarities because of too many relevant parameters [Eq. (4)]. In practice, the physical studies use a Froude similitude, but no systematic study was conducted to date to ascertain any scale effect affecting the turbulent mixing in tidal bore flows. The preceding analysis [Eq. (4)] does not account for the physio-chemical properties of the water, the air entrainment in the bore roller, or the characteristics of any intrusive instrumentation. This study focused on some basic laboratory experiments performed under controlled flow conditions in a relatively large size flume on the basis of a Froude similitude. The experimental configuration was selected to minimize potential viscous scaling effects by selecting large initial depths and velocities, and Reynolds numbers (Table 1).

Experimental Facility and Instrumentation

The experiments were performed in a 12-m long, 0.5-m wide tilting flume (Fig. 3). The channel was made of smooth PVC bed and glass walls. The water was supplied by a constant head tank to a large intake chamber with a smooth convergent feeding into the glass-walled channel. A fast-closing gate was located at the channel's downstream end. Two experimental configurations were tested. One series of experiments was conducted on the smooth PVC invert. For the other series of experiments, the bed was covered with plywood sheets covered by natural blue granite gravels, which were sieved 4.75–6.70 mm, glued in resin, and covered by a spray gloss surface finish. The hydraulic roughness of the gravel bed was tested in steady gradually varied flows, and the equivalent Darcy friction factor was $f = 0.036$ on average, corresponding to an equivalent sand roughness height $k_s = 3.4$ mm. Table 1 shows the range of experimental flow conditions for the free-surface measurements where Q is the initially steady flow rate and S_o is the bed slope. For $1.4 < F < 1.6$, the flow conditions corresponded to a 5:1 scale study of the bore shown in Fig. 1.

The flow rate was measured with two orifice meters that were calibrated on site with a volume per time technique. In steady flows, the water depths were measured using rail-mounted pointer gauges.

Table 1. Free-Surface Properties of Tidal Bores (in This Study)

Bed roughness	Q(m^3/s)	S_o	d_o[a] (m)	F	R	Type of tidal bore	d_{conj}/d_o	d_{max}/d_o	a_w/d_o	a_w/L_w
Smooth PVC bed	0.050	0	0.119	1.65	1.9×10^5	Breaking	1.88	Not available	Not available	Not available
			0.117	1.59	1.8×10^5	Breaking	1.93	Not available	Not available	Not available
			0.117	1.44	1.8×10^5	Undular/breaking	1.58	1.72	0.141	0.018
			0.117	1.36	1.7×10^5	Undular	1.45	1.71	0.234	0.032
			0.116	1.24	1.5×10^5	Undular	1.36	1.61	0.186	0.027
			0.117	1.11	1.4×10^5	Undular	1.22	1.33	0.096	0.013
			0.117	1.08	1.3×10^5	Undular	1.10	1.18	0.074	0.005
Fixed gravel bed	0.050	0.002	0.125[b]	1.52	1.6×10^5	Undular/breaking	1.71	1.93	0.193	0.028
			0.125[b]	1.45	1.6×10^5	Undular	1.48	1.75	0.280	0.040
			0.125[b]	1.40	1.5×10^5	Undular	1.48	1.77	0.285	0.046
			0.125[b]	1.24	1.4×10^5	Undular	1.32	1.45	0.149	0.019
			0.125[b]	1.17	1.3×10^5	Undular	1.23	1.29	0.069	0.008
			0.125[b]	1.01	1.1×10^5	Undular	1.13	1.13	0.023	0.001

Note: a_w = wave amplitude of first wave length; d_o = initial water depth; d_{conj} = conjugate depth; d_{max} = water depth of first wave crest; F = tidal bore Froude number; L_w = first wave length; Q = discharge; R = bore Reynolds number; S_o = bed slope; all data were recorded at $x = 5$ m.
[a]Measured at $x = 5$ m.
[b]Measured above the roughness.

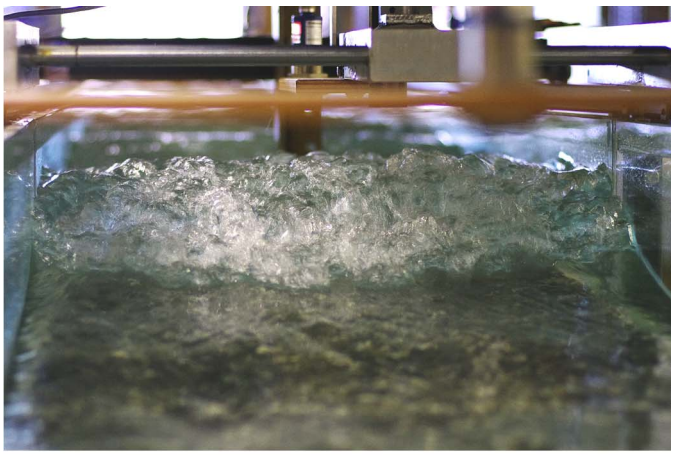

(a)

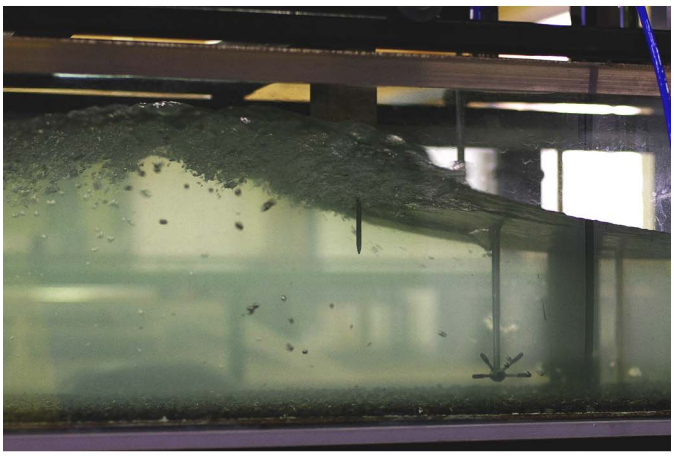

(b)

Fig. 3. Breaking tidal bores in the laboratory channel: (a) looking downstream at the advancing breaking bore roller: $Q = 0.050$ m^3/s, $d_o = 0.120$ m, F = 1.58, R = 2.0×10^5, fixed gravel bed, shutter = 1/60 s; (b) bore propagation from left to right: $Q = 0.050$ m^3/s, $d_o = 0.125$ m, F = 1.5, R = 1.9×10^5, fixed gravel bed, shutter = 1/100 s; an underwater bubble "trail" is behind the bore roller on the left and an acoustic Doppler velocimeter head is on the right

The unsteady water depths were recorded using several acoustic displacement meters (Microsonic Mic+25/IU/TC) with an accuracy of 0.2 mm. The turbulent velocity measurements were performed with an acoustic Doppler velocimeter (ADV) (Nortek Vectrino+) equipped with a three-dimensional side-looking head [Fig. 3(b)]. The velocity range was set to 1.0 m/s, and the data accuracy was 1% of velocity range (i.e., 0.01 m/s). The translation of the ADV probe in the vertical direction was controlled by a fine adjustment traveling mechanism connected to a Mitutoyo digimatic scale unit with an error less than 0.1 mm. All of the measurements were taken on the channel centerline, and the ADV and displacement sensors were synchronized within 1 ms and sampled simultaneously at 200 Hz.

During some preliminary experiments, recurrent problems were observed with the velocity data, including low correlations and low signal-to-noise ratios, because of the inadequate seeding of the channel water. Thereafter, and for the entire study, the channel water was seeded with 100 g of clay powder per hour of operation. The clay powder was introduced in the intake structure and was dispersed progressively with time. Further more, the unsteady flow postprocessing was limited to removal of communication errors following Koch and Chanson (2009) and Chanson (2010), and it is acknowledged that the vertical velocity component Vz data may be affected adversely by the bed proximity for $z < 0.030$ m. This is further discussed and documented in Docherty and Chanson (2010), together with more detailed information on the experimental apparatus.

Inflow Conditions and Tidal Bore Generation

For each experimental run, the initially steady flow conditions were established for 5 min before the first measurements. The tidal bore was generated by the rapid partial closure of the downstream gate. The gate closure time was less than 0.15 s. After closure, the bore propagated upstream (Fig. 3), and each experiment was stopped before the bore front reached the channel upstream end to avoid any wave reflection effect. The ADV measurements were conducted at $x = 5$ m downstream of the channel upstream end. In steady flows, some detailed velocity measurements indicated that the flow was partially developed at $x = 5$ m; $\delta/d_o = 0.47$ and 0.64 for smooth bed and fixed gravel bed, respectively.

For each series of experiments, the free-surface properties were documented (Table 1). Then some detailed velocity measurements were conducted in breaking bores at $x = 5$ m for $0.005 < z/d_o < 0.77$. On the gravel bed, z was measured above the top of the gravel materials using a semicircular footing with a 25.1-cm^2 area. At a number of vertical elevations, a series of 20 instantaneous velocity records were repeated with the same well-defined initially steady flow conditions. An ensemble median of each instantaneous velocity component was calculated.

Free-surface Measurements

The free-surface observations highlighted two types of tidal bores depending on the Froude number F. For a Froude number between unity and 1.5, the tidal bore was undular; that is, the tidal bore front was followed by a train of secondary, quasi periodic waves called undulations. For larger Froude numbers (F > 1.5–1.6), a breaking bore with a marked roller was observed (Fig. 3). The findings were identical for smooth and rough bed, and they were comparable with those of earlier studies (Treske 1994; Hornung et al. 1995; Koch and Chanson 2009).

For tidal bore Froude numbers less than 1.5, the bore consisted of a first wave followed by a train of well-formed undulations. The wave amplitude a_w and steepness a_w/L_w data are shown in Table 1, together with the conjugate depth d_{conj} and maximum water depth d_{max} at the first wave crest. The dimensionless wave steepness data are shown in Fig. 4. In Fig. 4, the data were compared with laboratory observations and with the linear wave theory solution of Lemoine (1948) and the Boussinesq's equation solution of Andersen (1978). For a bore Froude number slightly larger than unity, the wave steepness increased monotically with an increasing Froude number F to a local maximum followed by a sharp decrease immediately before the disappearance of free-surface undulations. The observations were consistent with earlier data, as shown in Fig. 4.

For a tidal bore with a marked roller (F = 1.5 − 1.6), the visual observations showed that the flow was basically two-dimensional, and the free-surface properties were systematically investigated by repeating 25 identical experiments with the results ensemble averaged (EA) (Fig. 5). The flow conditions could be considered as a 5:1 scale study ($L_r = 5$) of the tidal bore shown in Fig. 1. Both the free-surface and the visual observations showed that the free-surface elevation rose first slowly, immediately before the roller (Figs. 5 and 6). This is shown in Fig. 6, where the period Δt_1 corresponded to the duration of the gentle rise h_s of the free-surface, with $h_s/d_o \asymp 0.1$ (Table 2). Such a gradual rise in free surface ahead of the turbulent roller was previously observed by Hornung et al. (1995) and Koch and Chanson (2009). Immediately after, the turbulent roller caused by a sharp rise in water depth that was basically a discontinuity (Fig. 5). This corresponded to the period Δt_2 shown in Fig. 6. The characteristic free-surface length and time scale data are shown in Table 2.

Fig. 5 shows the time variations of the EA median water depth and fluctuations for both smooth and gravel beds. Each graph includes the EA median water depth d_{median} and the differences between 3rd and 4th quartiles ($d_{75} - d_{25}$) and 90 and 10% percentiles ($d_{90} - d_{10}$). Both ($d_{75} - d_{25}$) and ($d_{90} - d_{10}$) characterized the

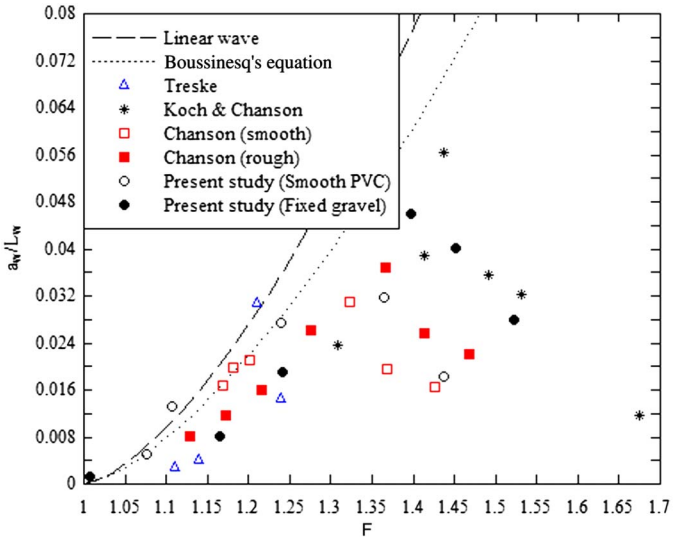

Fig. 4. Dimensionless wave steepness a_w/L_w as a function of the undular tidal bore Froude number; comparison between the present undular bore data, earlier laboratory studies (Treske 1994; Koch and Chanson 2009; Chanson 2010), linear wave theory (Lemoine 1948) and Boussinesq's equation (Andersen 1978)

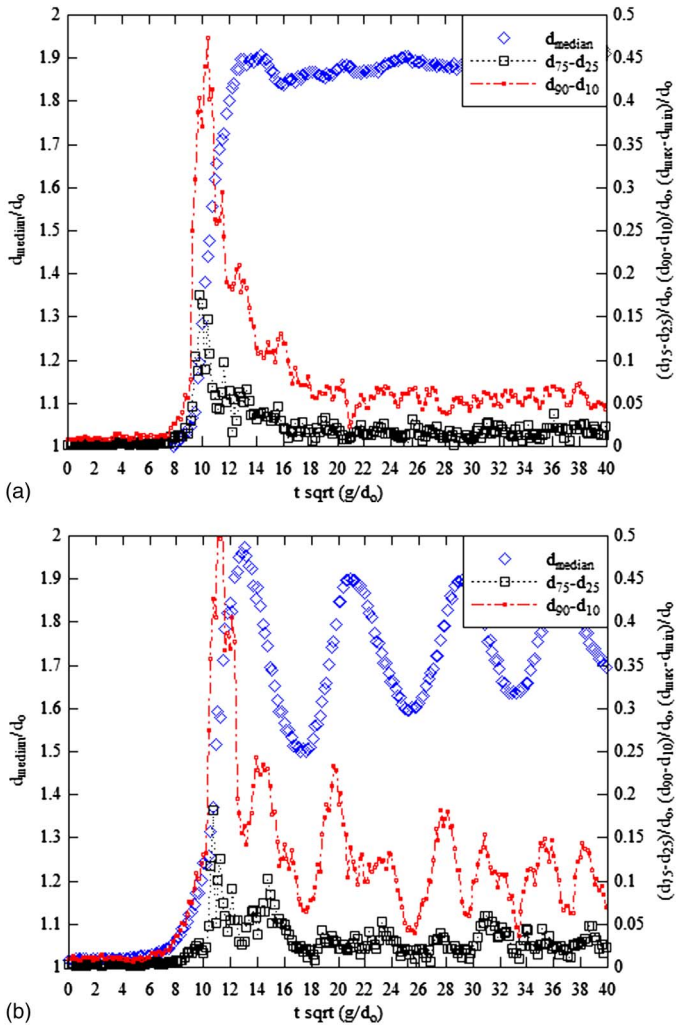

Fig. 5. Ensemble-averaged median water depth d_{median}, difference between 3rd and 4th quartiles ($d_{75} - d_{25}$), and difference between 90 and 10% percentiles ($d_{90} - d_{10}$) in a breaking tidal bore: (a) F = 1.65, R = 2.1×10^5, $Q = 0.0499$ m^3/s, $d_o = 0.119$ m, smooth PVC bed data; (b) F = 1.50, R = 1.7×10^5, $Q = 0.0500$ m^3/s, $d_o = 0.127$ m, fixed gravel bed data

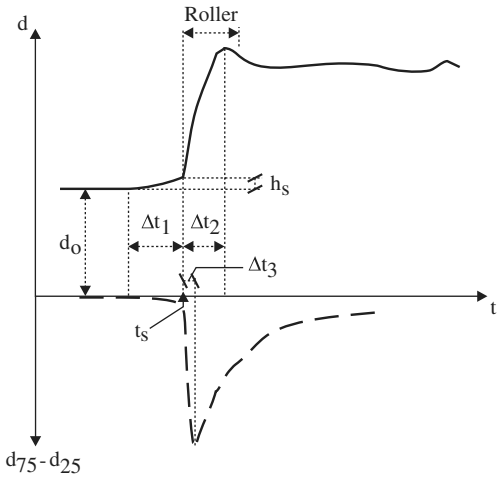

Fig. 6. Sketch of median and fluctuations of water depth in a breaking bore front

free-surface fluctuations around the median value. The data showed that the free-surface fluctuations were the largest next to the roller toe and impingement point, and they decayed quasi exponentially with increasing time as the bore roller passed beneath the sensor. Typically, the maximum free-surface fluctuations were observed during the first half of the bore roller with $\Delta t_3/\Delta t_2 = 0.48$ (Fig. 5), and the observation was consistent with the findings of Mouaze et al. (2005) and Murzyn and Chanson (2009) in stationary hydraulic jumps.

Unsteady Velocity Measurements

In a tidal bore with a marked roller, the turbulent velocity measurements showed that the arrival of the tidal bore and the sudden increase in water depth yielded a rapid change in the longitudinal velocity component to satisfy the conservation of mass. The longitudinal velocities were characterized by a rapid flow deceleration at all vertical elevations, whereas some large fluctuations of longitudinal, transverse, and vertical velocity components were observed beneath the tidal bore. The tidal bore was a hydrodynamic shock characterized by a sudden change in the velocity field (Lighthill 1978). The front was followed by a very turbulent flow motion with significant fluctuations of all velocity components. Some typical Euler measurements are shown in Fig. 7. Fig. 7 shows the instantaneous free-surface elevation, longitudinal, and vertical velocity components as function of time.

An ensemble median of each instantaneous velocity component was produced at selected vertical elevations. Some typical results are shown in Fig. 7 and compared with the instantaneous data for an experiment (Run 1). Both the instantaneous and EA data showed some key features of the unsteady turbulence in breaking tidal bores. These included a rapid flow deceleration during the passage of the tidal bore roller above the sampling volume; some negative longitudinal velocity component next to the bed [Figs. 7(a) and 7(b)], highlighting some transient recirculation "bubble"; and some positive vertical velocity component beneath the roller [Figs. 7(c) and 7(d)]. The latter was believed to be closely linked with the streamline curvature immediately before the bore roller.

The experimental results showed that the passage of the roller was associated with some large free-surface fluctuations (Fig. 5) and linked with some large longitudinal velocity fluctuations and some transient upward flow motion ($V_z > 0$) (Fig. 8). Fig. 8 shows the differences between the 3rd and 4th quartiles ($V_{75} - V_{25}$) and 90 and 10% percentiles ($V_{90} - V_{10}$) for the longitudinal and transverse velocity components, which gave a measure of the turbulent velocity fluctuations. The maximum horizontal velocity fluctuations occurred about the same time as when the maximum free-surface fluctuations were observed. Furthermore, the transverse velocity data V_y presented some large fluctuations after the bore front for $z/d_o \geq 0.43$, typically five to 10 times $\sqrt{g/d_o}$ after the front passage [Fig. 8(b)]. The findings implied some intense secondary motion in the wake of the tidal bore front.

Interestingly, the vertical velocity data V_z presented a substantial positive value during the front passage for $z/d_o \geq 0.43$ [Figs. 7(c) and 7(d)]. It is believed to be closely linked with the streamline curvature immediately before the bore roller ($t < t_s$) and possibly during the roller propagation. Because the free-surface is streamline, the surface slope is related to the vertical velocity component at the free-surface

$$\frac{V_z(z=d)}{V_x(z=d)} = \frac{\partial d}{\partial x} \tag{5}$$

where $V_x(z = d)$ = horizontal velocity component at the surface; and, at the bed, $V_z(z = 0) = 0$ for an impervious boundary. For a solitary wave, Boussinesq (1871) assumed a linear distribution of vertical velocity

$$\frac{V_z}{V_z(z=d)} = \frac{z}{d} \tag{6}$$

The result may be applied to open channel flows with streamline curvature (Montes 1998). In this study, the magnitude of the maximum median vertical velocity component $(V_z)_{max}$ increased with increasing distance from the bed [Figs. 7(c) and 7(d)]. Fig. 9 shows

Table 2. Breaking Bore Free-Surface Elevation Time and Length Scale (Breaking Tidal Bore on Horizontal Channel)

Reference	Q (m^3/s)	d_o[a] (m)	F	Bed roughness	h_s/d_o	$\sqrt{\frac{g}{d_o}}\Delta t_1$	$\sqrt{\frac{g}{d_o}}\Delta t_2$	$\sqrt{\frac{g}{d_o}}\Delta t_3$
Koch and Chanson (2009)	0.040	0.079	1.75–1.9	Smooth PVC	0.10	—	—	—
Chanson (2010)	0.058	0.137	1.50	Smooth PVC	0.116	2.71	2.03	—
		0.142[c]	1.46	Plastic screens ($k_s = 6.6$ mm)	0.107	3.41	2.16	—
This study[b]	0.050	0.119	1.65	Smooth PVC	0.080	3.18	4.36	1.63
		0.127[c]	1.50	Fixed gravel bed ($k_s = 3.4$ mm)	0.150	2.81	3.16	1.93

[a]Measured at $x = 5$ m.
[b]Ensemble-averaged data.
[c]Measured above the roughness.

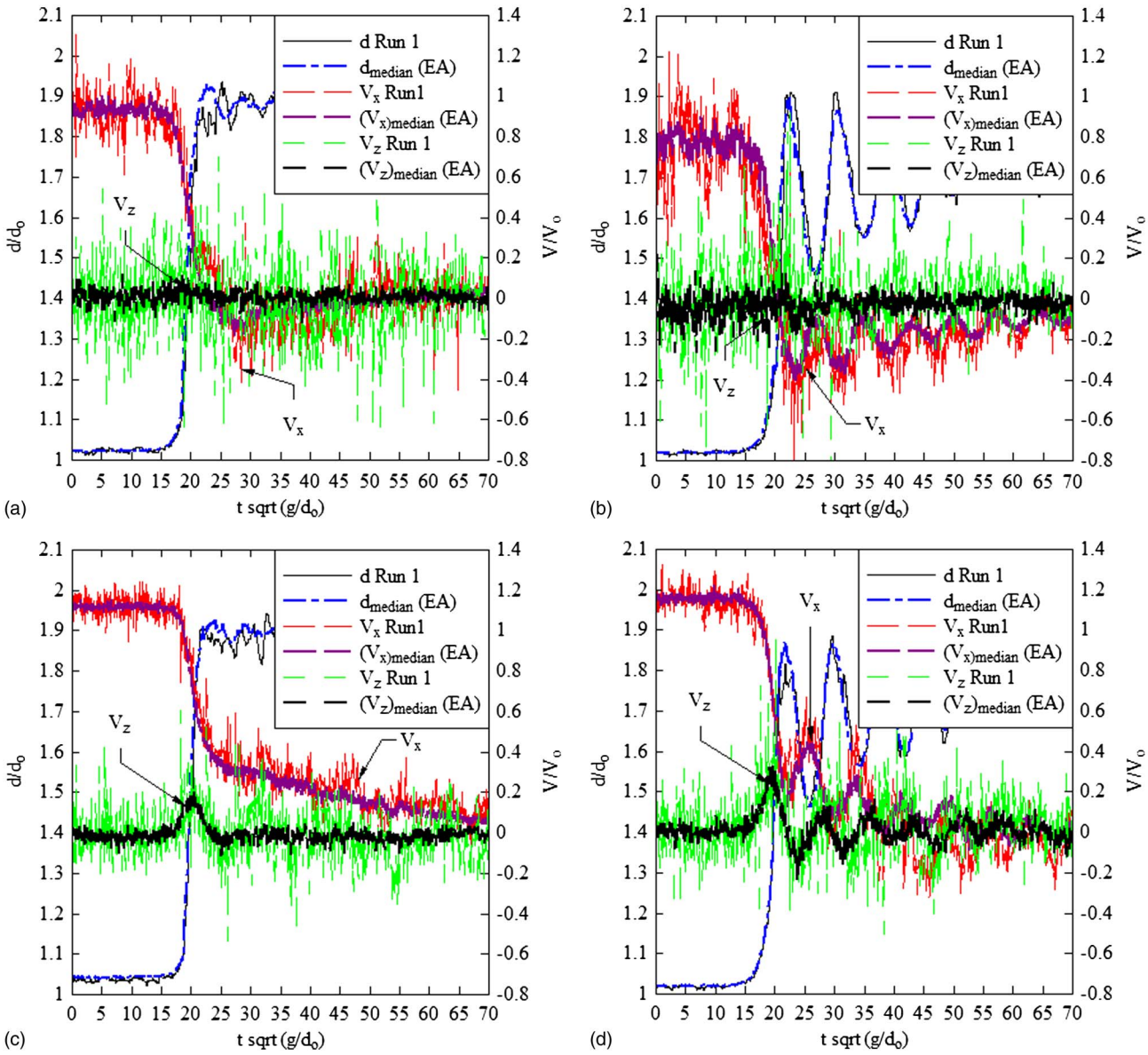

Fig. 7. Free-surface and turbulent velocity measurements under breaking tidal bore; flow conditions: (a and c) smooth PVC bed, $F = 1.6$, $R = 2.0 \times 10^5$, $d_o = 0.118$ m, $Q = 0.050$ m^3/s; (b and d) fixed gravel bed, $F = 1.5$, $R = 2.1 \times 10^5$, $d_o = 0.126$ m, $Q = 0.050$ m^3/s; (a–d) $z/d_o = 0.134$, 0.135, 0.733, and 0.733, respectively

the maximum median vertical velocity component as a function of the vertical elevation. On the same graph, the free-surface elevation rate $(\partial d/\partial t)_{z=d}$ is also shown. Because $V_z(z=0) = 0$ at the bed and $V_z(z=d) = (\partial d/\partial t)_{z=d}$ at the free-surface, an entire data trend can be extrapolated; the data were best correlated by

$$\left(\frac{V_z}{V_o}\right)_{\max} = 0.215 \times \frac{z}{d_o} \quad \text{for } 0 < z/d < 1 \text{ on smooth PVC} \quad (7)$$

$$\left(\frac{V_z}{V_o}\right)_{\max} = 0.466 \times \left(\frac{z}{d_o}\right)^{1.54} \quad \text{for } 0 < z/d < 1 \text{ on fixed gravel} \quad (8)$$

with a normalized correlation coefficient of 0.982 and 0.999 for Eqs. (7) and (8), respectively [Fig. 9]. The smooth bed data [Eq. (7)] corresponded to Boussinesq's (1871) approximation [Eq. (6)], and the gravel bed data yielded a similar monotonic relationship but with a different power law exponent [Eq. (8), Fig. 9].

Discussion

The experimental results highlighted simply a quantitative difference between the smooth and rough beds in the initially steady flow and during the unsteady bore motion, as seen in Fig. 6. These differences may be linked with slightly different flow conditions (Table 1) but may also be associated with some effects of the bed roughness on the turbulent flow field, especially close to the bed.

The results showed that the passage of a breaking bore is characterized by large turbulent velocity fluctuations at all vertical elevations, including next to the bed (Fig. 6). When the breaking tidal bore propagates upstream in a river, the natural riverbed is subjected to a rapid flow reversal during the transient recirculation,

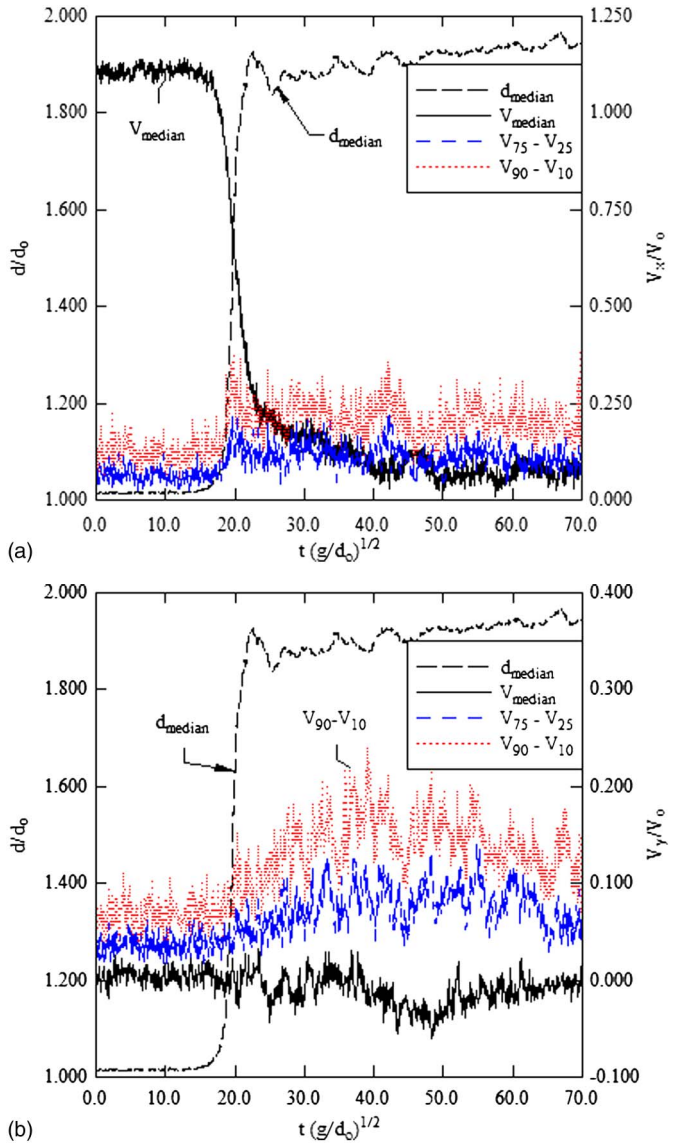

Fig. 8. Ensemble-average median velocity component V_{median}, difference between 3rd and 4th quartiles ($V_{75} - V_{25}$) and 90 and 10% percentiles ($V_{90} - V_{10}$), and ensemble-average median water depth $d_{\text{median}} - Q = 0.050\ \text{m}^3/\text{s}$, $d_o = 0.117$ m, $\mathsf{F} = 1.6$, $\mathsf{R} = 2.0 \times 10^6$, $z/d_o = 0.434$, smooth PVC bed: (a) longitudinal velocity component V_x; (b) transverse velocity component V_y

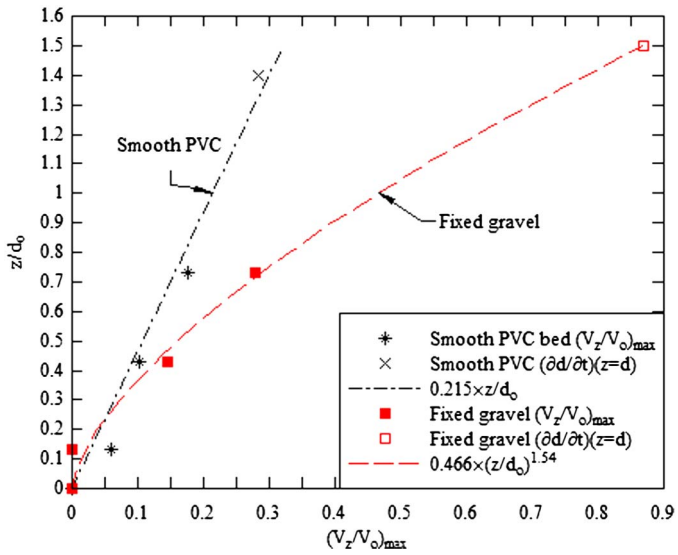

Fig. 9. Maximum median vertical velocity beneath the tidal bore roller and corresponding free-surface vertical velocity on smooth PVC and fixed gravel beds; flow conditions: (a) smooth PVC bed, $\mathsf{F} = 1.6$, $\mathsf{R} = 2.0 \times 10^5$, $d_o = 0.118$ m, $Q = 0.050\ \text{m}^3/\text{s}$; (b) fixed gravel bed, $\mathsf{F} = 1.5$, $\mathsf{R} = 2.1 \times 10^5$, $d_o = 0.126$ m, $Q = 0.050\ \text{m}^3/\text{s}$; comparison with Eqs. (7) and (8)

associated with large fluctuations of all velocity components (Figs. 7 and 8) beneath and behind the bore roller. Next to the bed, the large velocity gradients associated with the velocity fluctuations induce some large turbulent shear stresses, and the bed is subjected to significant velocity reversals associated with some cyclic loading. The natural bed material consists typically of cohesive sediments, which are saturated, and the changes in pore pressures may induce some liquefaction, contributing to the upward advection of bed material into the water column. The advected material is then transported upstream by the breaking bore [Fig. 2(b)]. Fig. 2(b) shows a sketch of the natural bed scour behind a breaking tidal bore.

These findings highlighted the drastic effect of a tidal bore onto the estuarine process. In turn, any artificial intervention leading to the disappearance of the tidal bore may have adverse effects on the natural ecosystem. For example, the bores of the Seine and Couesnon Rivers in France no longer exist after extensive training works and dredging and the construction of upstream barrage, respectively (Chanson 2011).

Conclusions

The unsteady turbulence in tidal bores was investigated physically under controlled conditions with two types of bed roughness: smooth PVC and fixed gravel bed. Some free-surface measurements were conducted with tidal bore Froude numbers of 1–1.7. Both undular and breaking bores were observed. The tidal bore flow patterns were independent of the bed roughness. The free-surface properties were close to earlier findings. Using an EA technique, the free-surface fluctuations of breaking tidal bores were characterized. Immediately before the roller, the free-surface curved gradually upward, and the gentle surface elevation rise was approximately $0.1d_o$, where d_o is the initial water depth. The passage of the bore roller was associated with some large water depth fluctuations; the largest free-surface fluctuations were observed during the first half of the bore roller.

Some detailed turbulent velocity measurements were performed at several vertical elevations during and shortly after the passage of breaking bores. Both the instantaneous and EA velocity data highlighted some seminal features. That is, a strong flow deceleration was observed at all elevations during the tidal bore passage. Close to the bed, the longitudinal velocity component became negative immediately after the roller passage, implying the existence of a transient recirculation. The height and duration of the transient was a function of the bed roughness, with a higher and longer recirculation region above the rough bed. The vertical velocity data presented some positive, upward motion during the bore passage, with increasing maximum vertical velocity with increasing distance from the bed. The vertical motion was believed to be linked with some streamline curvature in front of the roller. The transverse velocity data presented some large fluctuations with nonzero EA

after the roller passage, which highlighted some intense secondary motion advected behind the bore.

Acknowledgments

The authors thank Graham Illidge and Clive Booth (University of Queensland, Australia) for their technical assistance. They thank further Prof. Colin Apelt (University of Queensland, Australia), Prof. Laurent David (University of Poitiers, France), and Dr David Reungoat (University of Bordeaux, France) for their valuable comments.

Notation

The following symbols are used in this paper:

a_w = wave amplitude (m);
B = channel width (m);
d = (a) flow depth (m) measured normal to the invert; (b) flow depth (m) measured above the fixed gravel bed;
d_{conj} = conjugate flow depth (m) measured immediately behind the tidal bore front;
d_{max} = flow depth (m) at the first wave crest;
d_o = initial flow depth (m) measured normal to the chute invert;
F = tidal bore Froude number, defined as $\mathsf{F} = (V_o + U)/\sqrt{g \times d_o}$;
f = Darcy-Weisbach friction factor;
g = gravity constant (m/s^2); $g = 9.80$ m/s^2 in Brisbane, Australia;
h_s = rise in free-surface elevation (m) in front of the breaking bore front (Fig. 6);
k_s = equivalent sand roughness height (m);
L_r = geometric scaling ratio;
L_w = wave length (m) measured from crest to crest;
Q = volume flow rate (m^3/s);
R = tidal bore Reynolds number; $\mathsf{R} = \rho(V_o + U)d_o/\mu$;
S_o = bed slope; $S_o = \sin\theta$;
t = time (s);
U = tidal bore front celerity (m/s) for an observer standing on the bank, positive upstream;
V_o = initial flow velocity (m/s) positive downstream; $V_o = q/d_o$;
V_x = longitudinal velocity (m/s) positive downstream;
V_y = transverse velocity (m/s) positive toward the left sidewall;
V_z = vertical velocity (m/s) positive upward;
x = longitudinal distance (m) measured from the channel upstream end, positive downstream;
y = transverse distance (m) measured from the channel centerline, positive toward the left sidewall;
z = distance (m) normal to the bed; it is the vertical distance (m) for a horizontal channel; for a fixed gravel bed, z is measured above the top of the gravel bed;
Δt_1, Δt_2, Δt_3 = characteristic periods (s) of the breaking bore front (Fig. 6);
δ = boundary layer thickness (m) defined in terms of 99% of the free-stream velocity;
μ = dynamic viscosity (Pa.s);
θ = bed slope angle with the horizontal, positive downwards;
ρ = water density (kg/m^3);
σ = surface tension between air and water (Pa.s); and
$\partial/\partial z$ = partial differentiation with respect to z.

Subscripts

conj = conjugate flow conditions (i.e., immediately behind the tidal bore front);
median = median value (i.e., 50% percentile);
x = longitudinal component positive downstream;
y = component transverse to the channel centerline;
z = component normal to the invert; and
o = initial flow conditions (i.e., upstream of the positive surge front);
10 = 10% percentile;
25 = 25% percentile;
75 = 75% percentile; and
90 = 90% percentile.

References

Andersen, V. M. (1978). "Undular hydraulic jump." *J. Hydraul. Div.*, 104(8), 1185–1188.

Boussinesq, J. V. (1871). "Théorie de l'intumescence appelée onde solitaire ou de translation se propageant dans un canal rectangulaire." *Comptes-Rendus de l'Académie des Sciences*, Vol. 72, Paris, 755–759 (in French).

Chanson, H. (1999). *The hydraulics of open channel flow: An introduction*, Edward Arnold, London.

Chanson, H. (2010). "Unsteady turbulence in tidal bores: Effects of bed roughness." *J. Waterway, Port, Coastal, Ocean Eng.*, 136(5), 247–256, 10.1061/(ASCE)WW.1943-5460.0000048.

Chanson, H. (2011). *Tidal bores, aegir, eagre, mascaret, pororoca: Theory and observations*, World Scientific, Singapore.

Chanson, H. (2012). "Momentum considerations in hydraulic jumps and bores." *J. Irrig. Drain. Eng.*, 138(3), 10.1061/(ASCE)IR.1943-4774.0000409.

Docherty, N. J., and Chanson, H. (2010). "Characterisation of unsteady turbulence in breaking tidal bores including the effects of bed roughness." *Hydraulic Model Rep. No. CH76/10*, School of Civil Engineering, Univ. of Queensland, Brisbane, Australia.

Henderson, F. M. (1966). *Open channel flow*, MacMillan Company, New York.

Hornung, H. G., Willert, C., and Turner, S. (1995). "The flow field downstream of a hydraulic jump." *J. Fluid Mech.*, 287, 299–316.

Koch, C., and Chanson, H. (2009). "Turbulence measurements in positive surges and bores." *J. Hydraul. Res.*, 47(1), 29–4010.3826/jhr.2009.2954.

Lemoine, R. (1948). "Sur les ondes positives de translation dans les canaux et sur le ressaut ondulé de.aible amplitude." *Houille Blanche*, 2, 183–185 (in French).

Liggett, J. A. (1994). *Fluid mechanics*, McGraw-Hill, New York.

Lighthill, J. (1978). *Waves in fluids*, Cambridge University Press, Cambridge, U.K.

Montes, J. S. (1998). *Hydraulics of open channel flow*, ASCE Press, New York.

Mouaze, D., Murzyn, F., and Chaplin, J. R. (2005). "Free surface length scale estimation in hydraulic jumps." *J. Fluids Eng.*, 127(6), 1191–1193.

Murzyn, F., and Chanson, H. (2009). "Free-surface fluctuations in hydraulic jumps: Experimental observations." *Exp. Therm. Fluid. Sci.*, 33(7), 1055–1064, 10.1016/j.expthermflusci.2009.06.003.

Rayleigh, L. (1908). "Note on tidal bores." *Proc. R. Soc. London, Ser. A*, 81(541), 448–449.

Treske, A. (1994). "Undular bores (favre-waves) in open channels-experimental studies." *J. Hydraul. Res.*, 32(3), 355–370.